Appl. Phys. B 60, 95–102 (1995)

Applied Physics B Lasers and Optics

© Springer-Verlag 1995

One-electron parametric oscillator

C.H. Tseng, G. Gabrielse

Department of Physics, Harvard University, Cambridge, MA 02138, USA
(Fax: +1-617/495-0416, E-mail: GABRIELSE@husste.harvard.edu)

Received: 8 August 1994 / Accepted: 5 December 1994

Abstract. The parametric oscillation of a trapped electron is studied and used to measure enhanced spontaneous emission. Hysteresis in this motion provides a one bit memory to store information about excitations made with the electron "in the dark".

PACS: 42.65.–k

An electron in a Penning trap is typically observed by driving its axial motion along the magnetic-field direction with a driving force that is nearly resonant [1]. Instead, we modulate the trapping potential and thereby parametrically drive the electron's axial motion at approximately twice its resonant frequency. The magnitude and phase of the response are separately measured and compared to theoretical expectations, along with resonance line shapes, bistability and hysteresis, and the time required to excite to a steady state. These studies are done in extremely high vacuum, in an apparatus virtually identical to that used to establish a pressure less than 5×10^{-17} Torr [3], thereby avoiding the collisions which dominated an earlier observation [4]. Parametric resonance [2] is used to measure rapid, enhanced spontaneous emission for electron cyclotron motion in a trap cavity, at a rate too fast to have been measured previously. The bistability and hysteresis in parametric resonance is used to measure the cyclotron resonance frequency with a resolution of one part in 10^9, a resolution which corresponds to the relativistic shift in the cyclotron frequency caused by increasing the cyclotron quantum number by one. This resolution is attained while the electron is "in the dark" insofar as all nearly resonant drives (other than the cyclotron drive) and detectors are turned off, to avoid significantly increasing the electron's amplitude. Bistability and hysteresis in the parametric oscillator is used as a one-bit memory to record whether or not a cyclotron excitation occurs. "In the dark", detection should make it possible to increase the accuracy of tests of quantum electrodynamics which are already the most accurate comparison of physics experiment [5] and theory [6].

Dedicated to H. Walther on the occasion of his 60th birthday

1 Observed parametric resonance

One electron is stored at the center of the Penning trap represented in Fig. 1. Two end-cap electrodes, above and below, and a ring electrode, are shaped along the hyperbolic contours which are the equipotentials of the desired electrostatic quadrupole potential. An "orthogonalized" geometry [7] makes it possible to improve the shape of the trapping potential (by adjusting the potential on the asymptotic compensation electrodes) without changing the electron's oscillation frequencies. A 5.3 T magnetic field is directed along the vertical axis. An electron in this Penning trap undergoes the familiar motions [1] illustrated in Fig. 2. Throughout this paper, we shall assume that the slow magnetron motion (at frequency $\omega_m/2\pi = 13.6$ kHz) is cooled to essentially zero radius and is hence not an issue. The rapid cyclotron motion, also perpendicular to the magnetic-field direction, is at frequency $\omega_c'/2\pi = 148$ GHz. The axial motion, parallel to the magnetic-field direction, is at frequency $\omega_z/2\pi = 63.4$ MHz.

We focus on the axial motion of a single trapped electron for the rest of this section. The common way to monitor this motion is to drive one end cap near resonance at $\omega_d \approx \omega_z$ and detect the response voltage detected across the resistor R which is connected to the other end cap, as shown in Fig. 3. (We do not discuss a frequency modulation which is important for practical reasons but does not change the basic idea [1].) The measured points in Fig. 4a fit the expected Lorentzian line shape with a width of 12.2 Hz. The magnified residuals below in Fig. 4b clearly show that on resonance the electron "shorts out" the 4.2 K Johnson noise from the resistor. Figure 5 illustrates that it is also possible to detect a single electron without the external drive. The Johnson noise from the resistor is detected (the noise spectrum is not flat because of the pass band of a crystal filter) and the dip demonstrates again the "shorting" of this noise by the trapped electron. Such a dip is a common way to observe many trapped particles, but a very well-tuned trap and optimized electronics are needed to see a single trapped particle in this way. Figure 5 requires several minutes of averaging. The advantage is that an electron which is driven only by noise stays closer to the center of the trap where the electrostatic and magnetic field are most carefully controlled.

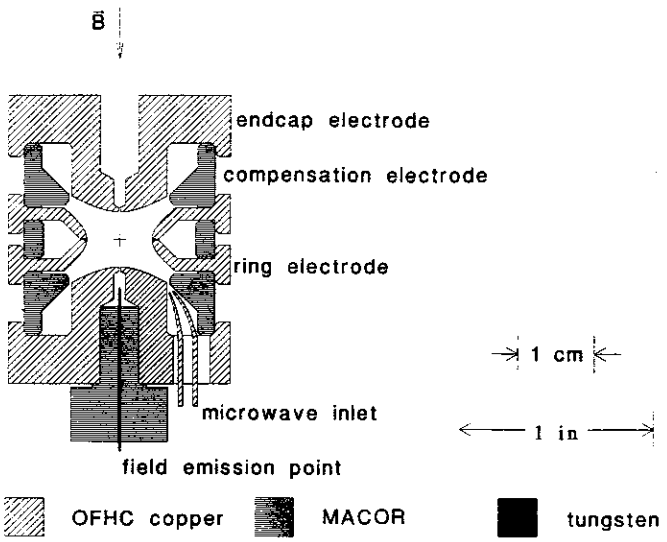

Fig. 1. Orthogonalized, hyperbolic Penning trap

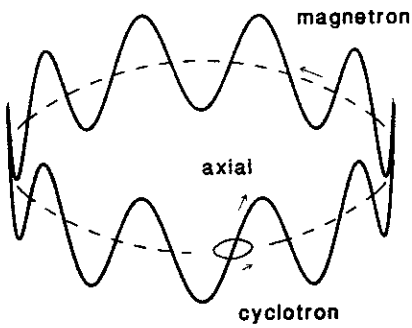

Fig. 2. Motion of one electron in a Penning trap (not to scale)

This paper demonstrates parametric resonance as a third way to detect the axial motion of a single trapped electron. (Detailed studies of the parametric resonance of many trapped electrons have been carried out [8].) Before the electron's axial motion is excited it experiences only a drive so far off the 12.2 Hz wide resonance, at $\omega_d/2\pi \approx 2\omega_z/2\pi \approx$ 127 MHz, that its oscillation amplitude does not increase because of the drive. In this sense, the electron remains "in the dark", because the drive does not make the electron oscillate further from the center of the trap. However, when the electron does come into parametric resonance, a large and easily observed axial oscillation at $\omega_d/2 \approx \omega_z$ is produced. In the next section, for example, we shift the electron's axial motion into parametric resonance with the drive using a cyclotron excitation, and measure how quickly a response occurs. The electron thus remains "in the dark" until a large signal is observed.

The setup in Fig. 3 produces a modulation of the trapping potential at ω_d as well as the direct drive mentioned previously. Such a parametric drive at frequency $\omega_d = 2(\omega_z + \epsilon)$ excites an electron oscillation at frequency $\omega_d/2 = \omega_z + \epsilon$. The one-electron, parametric oscillator has the equation of motion

$$\ddot{z} + \gamma_z \dot{z} + \omega_z^2(1 + h\cos\ \omega_d t)z + \lambda_4 z^3 + \lambda_6 z^5 = 0. \qquad (1)$$

The damping, at a rate $\gamma_z^{-1} = 0.013$ s, is due to energy dissipated in the detection resistor. Adjusting the compensation

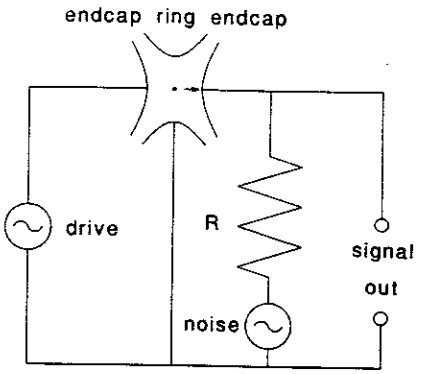

Fig. 3. Schematic circuit showing the drive and detection for an electron's axial motion

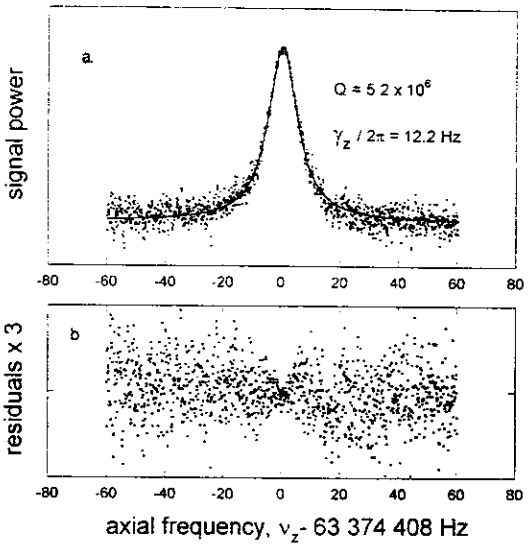

Fig. 4. a Response of an electron driven near its axial frequency (*points*) and a fit (*solid curve*) to the expected Lorentzian lineshape. **b** Residuals show clearly the effect of "noise shorting" on resonance

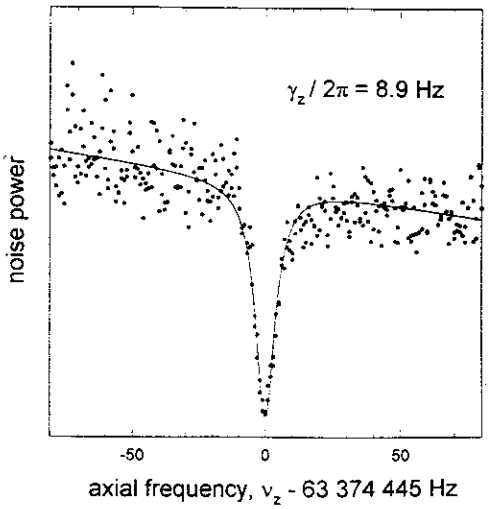

Fig. 5. Undriven (except by Johnson noise) electron shorts the Johnson noise from the 4.2 K resistor at frequencies near its axial resonance

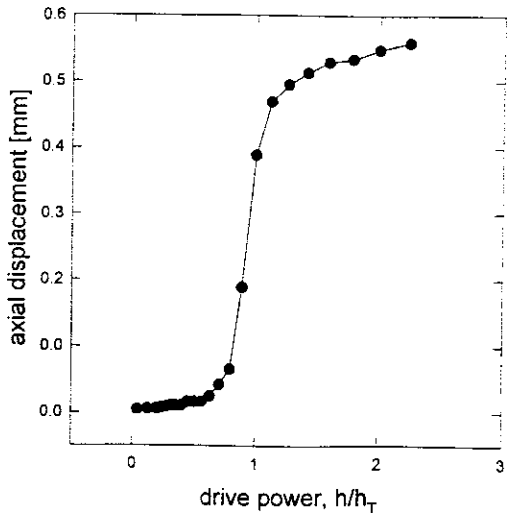

Fig. 6. Measured amplitude of the parametric response at ω_z undergoes an abrupt threshold as the strength h of the parametric drive at $\omega_d = 2\omega_z$ is increased

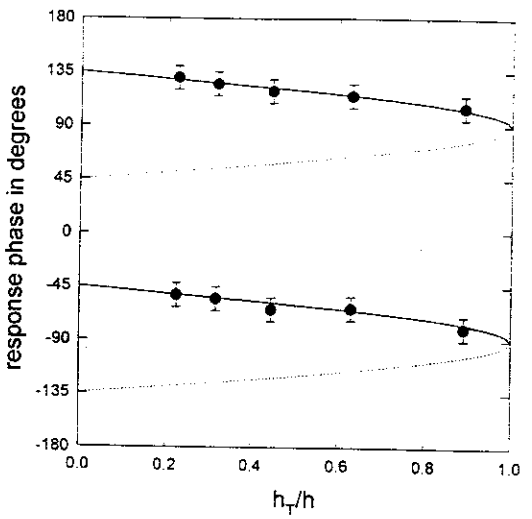

Fig. 7. Measured phase of the parametric response at $\omega_d/2 \approx \omega_z$ (*points*) vs the strength h of the drive, superimposed on the theoretical prediction of (3)

potential changes the coefficients λ_4 and λ_6 of the nonlinear terms. In terms of the Legendre expansion coefficients often used to describe Penning traps [1], $\lambda_4 = 2C_4/(1 + C_2)$ and $\lambda_6 = 3C_6/(1 + C_2)$.

If we start with no axial excitation ($z \approx 0$), and increase the drive strength h, the nonlinear terms are not important initially since z is small, and we thus have only the familiar Mathieu equation with damping. An abrupt threshold occurs when the effect of the drive overcomes the damping at drive strength $h = h_T$ with

$$h_T = 2\gamma_z/\omega_z = 3.8 \times 10^{-7}. \tag{2}$$

(The number to the right is the measured ratio.) This threshold is illustrated in Fig. 6 for a parametric drive resonant at $\omega_d = 2\omega_z$ (i.e., $\epsilon = 0$). Figure 7 compares the measured phase (points) and the calculated phase (curve) given by

$$\sin 2\Psi = h_T/h\ , \tag{3}$$

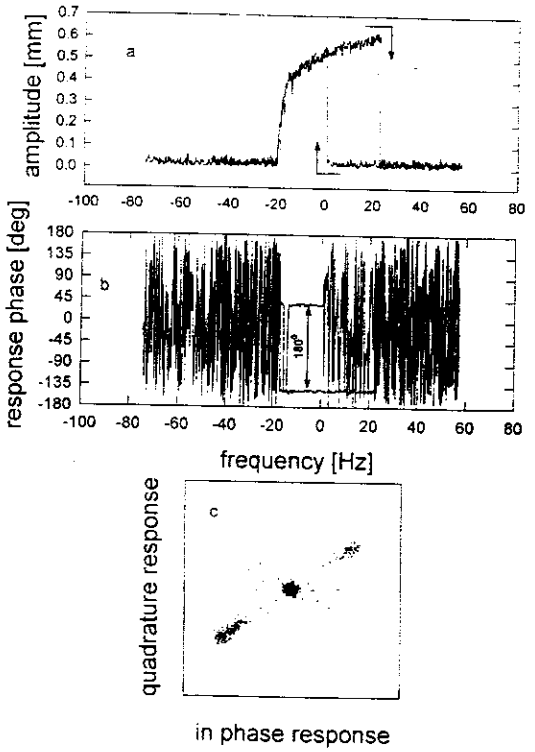

Fig. 8a–c. Amplitude (a) and phase (b) of the parametric response at $\omega_d/2 = \omega_z + \epsilon$ as the frequency of the parametric drive at ω_d is swept through resonance. The phase takes one of two bistable values near resonance and is not well defined off resonance where the response amplitude is very small, as is also illustrated in the measured phase-space plot in (c)

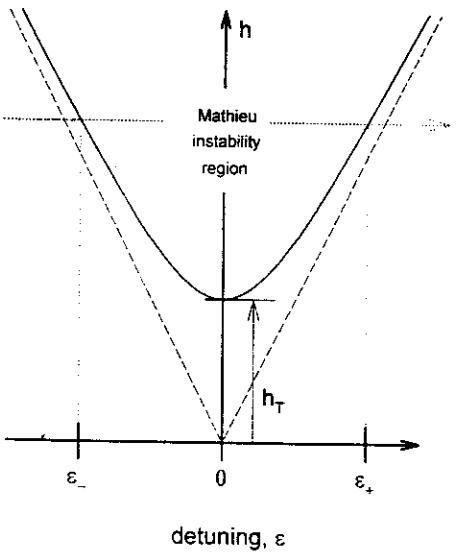

Fig. 9. Excitation range $\epsilon_+ - \epsilon_-$ vs parametric drive strength h for the Mathieu equation with damping

where Ψ is the relative phase between the response and the drive. The two solutions to this equation are separated by a phase of 180 degrees, corresponding to the timetranslation symmetry which occurs because the period of the driving force is half as long as the period of the response.

Figures 8a–c show the amplitude and phase response as the parametric drive is swept in frequency. The phase is

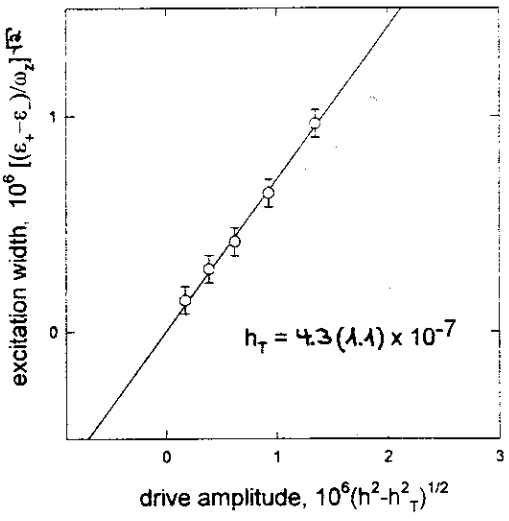

Fig. 10. Measured excitation range $\epsilon_+ - \epsilon_-$ vs parametric-drive amplitude

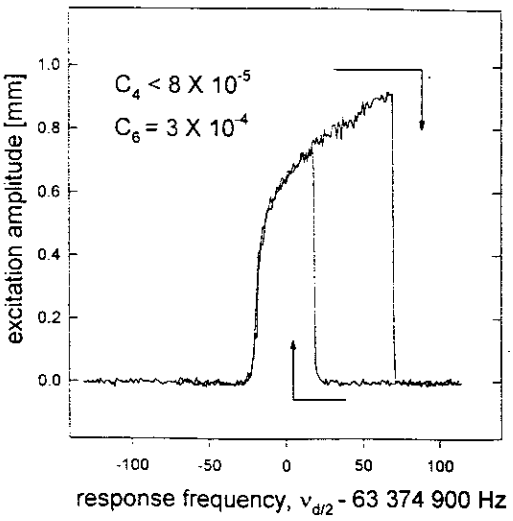

Fig. 11. Amplitude of the parametric response at $\omega_d/2 = \omega_z + \epsilon$ as the frequency of the parametric drive at ω_d is swept through resonance, when the trap is tuned to make C_4 as small as possible. (Calibration of the mm scale depends on a calculated parameter $D_4 = 8.7 \times 10^{-3}$ defined in [2])

not well defined until the axial motion is excited to a non-zero amplitude near resonance. Near resonance, either of the two phases separated by 180 degrees is equally likely. One example of each phase is superimposed in the figure, and the amplitude and phase of all measured points are also displayed in a polar, phase space plot. The sharply defined excitation range $\epsilon_- < \epsilon < \epsilon_+$ is a property of the damped Mathieu equation, with

$$\epsilon_\pm = \pm\frac{1}{4}\omega_z\sqrt{h^2 - h_T^2}. \tag{4}$$

(The nonlinearity keeps the motions from expanding exponentially without limit but does not effect the excitation range.) Figure 9 represents the excitation band $\epsilon_+ - \epsilon_-$ as a function of parametric drive amplitude. Figures 6 and 8a–c a correspond to vertical and horizontal slices through Fig. 9, respectively. Figure 10 shows the measured excitation range (points) as a function of the drive strengh, fit to (4) (curve). From this fit we obtain $h_T = 4.3(\pm 1.1) \times 10^{-7}$, in good agreement with (2).

The measured line shapes exhibit bistability and hysteresis, as illustrated in Fig. 11, where the line shape extends further when the drive is swept upward in frequency than when it is swept downward. The response in the double-valued bistable region thus depends on the excitation history. The trap was tuned in this case to make λ_4 as small as possible, and the observed shape is determined by the value of λ_6. If the trap is deliberately mistuned to make λ_4 much larger, the excited line shape then becomes a straight line, as is expected. If the trap is instead tuned so that both λ_4 and λ_6 are important, then a more complicated line shape results, one example of which is shown in Fig. 12. For parametric drives swept upward and downward through resonance, the measured amplitudes $A_\pm$ either vanish or lie on parallel parabolas

$$\frac{5\lambda_6\omega_z}{16}A_\pm^4 + \frac{3\lambda_4\omega_z}{8}A_\pm^2 + \epsilon_\pm - \epsilon = 0, \tag{5}$$

if we neglect higher-order nonlinearities than those mentioned. This fit makes it possible to determine both C_4 and C_6 (or equivalently λ_4 and λ_6). In following sections, we

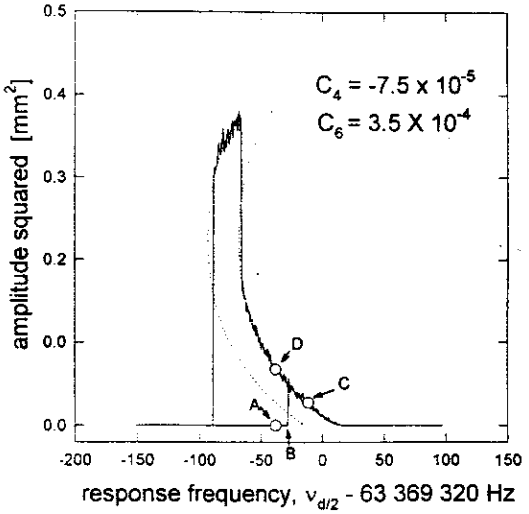

Fig. 12. Amplitude of the parametric response at $\omega_d/2 = \omega_z + \epsilon$ as the frequency of the parametric drive at ω_d is swept through resonance, when the trap is mistuned to increase C_4. The *dotted lines* are a fit to parallel parabolas given by (5)

will illustrate how to use the bistability and hysteresis to record information about an excitation made "in the dark".

So far, we have considered only the steady-state line shapes. It is important to realize, however, that the time it takes to reach the steady-state excitation amplitude depends upon the detuning ϵ of the drive from the resonant frequency. As the excitation begins from zero amplitude, the amplitude initially increases exponentially with the time constant τ given (within the excitation range) by

$$\tau^{-1} = \sqrt{\epsilon_\pm^2 - \epsilon^2 + (\gamma_z/2)^2} - \gamma_z/2, \tag{6}$$

which is determined solely by the damped Mathieu equation. As the amplitude increases, however, the nonlinearity becomes increasingly important and eventually arrests the exponential growth. Figure 13a, b illustrates how the re-

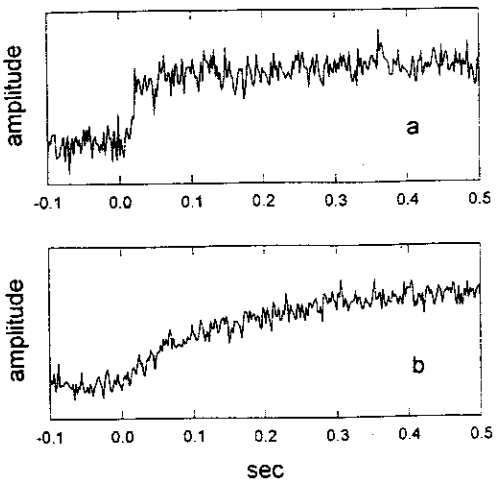

Fig. 13a, b. Amplitude of the parametric response at $\omega_z + \epsilon$ as a function of the time after the parametric drive at $2(\omega_z + \epsilon)$ was turned on at $t = 0$, for the faster resonant case of $\epsilon = 0$ in (**a**) and for a slower. non-resonant case of $\epsilon/2\pi = 20$ Hz in (**b**)

sponse amplitude grows as a function of time, with $t = 0$ being the time at which the parametric drive is turned on. The response grows much more quickly for a resonant drive, $\epsilon = 0$ in Fig. 13a, than for a non-resonant drive, $\epsilon/2\pi = 20$ Hz, in Fig. 13b. Note from (6) and (4) that the rise time within the excitation range can be decreased as desired by increasing the drive strength h and can be decreased by moving to the ends of the excitation range. The time taken to excite to a steady state will also depend in a very sensitive way upon the initial thermal excitation amplitude, suggesting excitation-time measurements as a promising way to measure axial temperature.

2 Cyclotron motion coupled to a cavity

The cyclotron oscillation frequency ω_c' is more than 2 000 times higher than the axial frequency ω_z. This motion can be excited with a very pure microwave drive [9] which enters the trap through the small tube shown in Fig. 1. A cyclotron excitation to energy E_c results in a shift in the axial frequency

$$\frac{\Delta\omega_z}{\omega_z} = -\frac{E_c}{2mc^2}, \tag{7}$$

and a shift in the cyclotron frequency

$$\frac{\Delta\omega_c'}{\omega_c'} = -\frac{E_c}{mc^2}. \tag{8}$$

Both of these shifts are due to special relativity and are often thought of as relativistic mass shifts since special relativity has the effect of replacing the mass m in the mass-dependent frequencies by γm, where γ is the familiar relativistic factor (the total energy, rest-mass energy plus kinetic energy, divided by the rest energy).

For the purposes of this paper, a cyclotron excitation simply causes the axial frequency to shift. The dip to the right in Fig. 14 is the undriven axial resonance observed for no cyclotron excitation. A cyclotron excitation of $E_c = 6.7$ eV causes the axial frequency to shift downward by 550 Hz (the left dip in Fig. 14). Turning off the cyclotron microwave drive causes the electron-resonance dip to shift back to its original position as the cyclotron motion spontaneously emits synchrotron radiation. This spontaneous emission is modified by the presence of a surrounding microwave cavity which can either enhance or inhibit the spontaneous emission [10, 11].

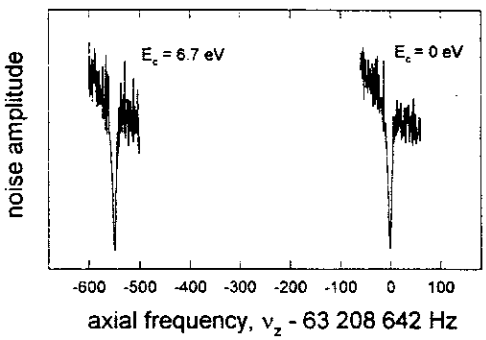

Fig. 14. Axial resonance of a single trapped electron (noise-shorting dip to the *right*) is shifted to a lower frequency (*left*) when the the electron's cyclotron motion is excited to an energy of E_c = 6.7 eV. When the cyclotron drive is turned off, the dip shifts back as the electron damps via its coupling to the radiation field in the trap cavity

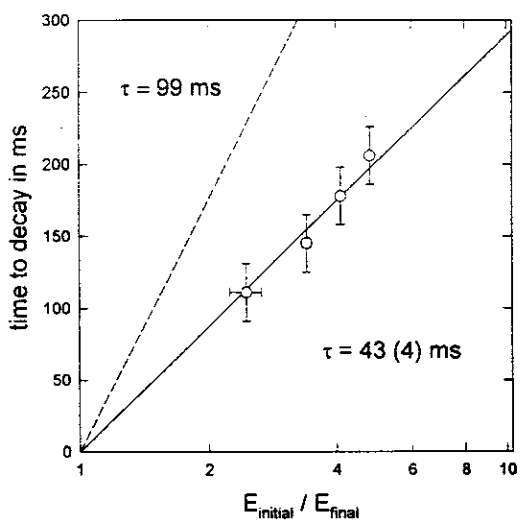

Fig. 15. Time between turning off the cyclotron drive and the first observation of a parametric axial response, as a function of the energy of the initial cyclotron excitation. The *fitted line* (constrained to pass through the origin) shows an exponential damping time for the cyclotron motion which is shorter than the spontaneous emission time in free space (*dashed line*). Spontaneous emission is enhanced by the coupling of the electron-cyclotron motion and the cavity

For the large cyclotron excitations used here, the time it takes the axial resonance to come within a line width of its $E_c = 0$ position is of order 100 ms. However, since it takes several minutes of signal averaging to observe the dip in the noise resonance, it is not possible to time resolve the shifting dip. One could apply a drive directly at ω_z for $E_c = 0$ and measure how long it takes to see the drive response illustrated in Fig. 4. Instead, we apply a parametric drive at $\omega_d = 2\omega_z$ and take advantage of the large signal which is rapidly produced by a parametric excitation. At time $t = 0$,

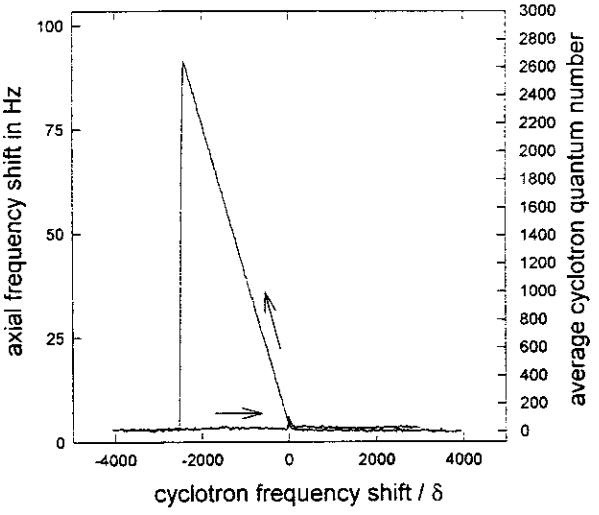

Fig. 16. Anharmonic cyclotron resonance with the anharmonicity due to special relativity

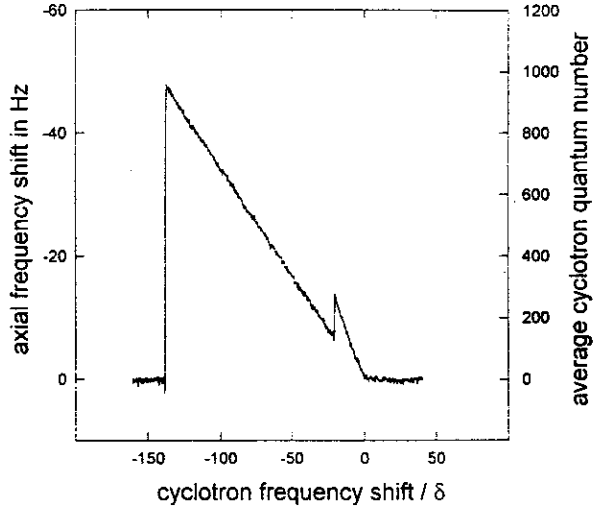

Fig. 17. Anharmonic cyclotron resonance for two electrons

the microwave drive is turned off and the cyclotron energy begins to damp. Special relativity shifts the axial resonance upward, eventually into parametric resonance with the drive. After a delay, a parametric response thus begins (much like those in Fig. 13a, b). The response grows with a time constant that is due to a filter included to improve the signal-to-noise ratio. When this filter is removed, we can observe rise times less than 10 ms but the signal-to-noise ratio is such that averaging over hours then becomes necessary. Figure 15 shows four measurements made of the time delay before a response is observed, for different values of the initial cyclotron excitation. Each point is an average of 10 trials. The fitted line (constrained to pass through the origin) gives an exponential damping time for the cyclotron motion of 43 ± 4 ms. In free space, this cyclotron radiation lifetime would be 99 ms. The spontaneous emission is clearly enhanced by the coupling between the cyclotron motion and the trap cavity. In the past, only the longer damping time for inhibited spontaneous emission could be observed [10].

During these measurements, we also observed the interesting behavior of two electrons whose cyclotron motions are excited. As a context, Fig. 16 shows the axial frequency of one electron as a cyclotron drive is swept downward (large shift) and upward (small excitation) through resonance. Like in earlier observations [9], the frequency of a driven and locked axial resonance is observed continuously. The characteristic, triangular resonant shape of the anharmonic oscillator is evident. This anharmonicity is due to special relativity, as stated in (8). Sweeping the cyclotron drive downward through resonance when two electrons are present in the trap exhibits a slightly more complicated resonance structure shown in Fig. 17. Initially, the slope is the same for two electrons as for one. This occurs because the center-of-mass motion is observed and the center of mass of two electrons has the same charge-to-mass ratio as does one electron. The cyclotron excitation energy drops suddenly but not to zero, presumably because one electron remains excited while the second damps to the center of the trap. The excitation of the excited electron continues and increases as the drive is swept downward in frequency until eventually this excitation also drops out. The measured ratio of the two slopes is 1.9 ± 0.2 and this ratio presumably could be calculated by considering an electron-cyclotron orbit perturbed by the presence of a second charge at the center of the orbit, though it may be necessary to consider small axial excitations as well. Related couplings of two antiprotons in cyclotron orbits with frequencies shifted by special relativity have been observed [12], as have similar couplings between a simultaneously trapped antiproton and H^- ion.

3 Measuring the cyclotron frequency "in the dark"

The measured enhanced spontaneous-emission rate reported in the last section was done "in the dark" insofar as the cyclotron decay occurred in the absence of any drive able to make an appreciable increase in the electron's excitation amplitude. However, the FET amplifier which detected the voltage induced across the resistor was left on continuously and energy dissipated in this FET caused the effective temperature of the resistor R to be higher than the ambient 4.2 K. We now consider a cyclotron-frequency measurement which is more "in the dark" insofar as the FET detection amplifier is turned off during the crucial part of the measurement, allowing the resistor temperature to decrease to the ambient 4.2 K. The parametric axial oscillator is used as a one-bit memory to record whether or not a cyclotron excitation occurred. Since special relativity produces a shift in the electron's axial frequency when the cyclotron motion is excited, we need only detect a shift in the axial frequency. A parametric drive is turned on at a frequency corresponding to point A in Fig. 12. The axial motion of the electron is not excited. A downward, relativistic shift in the electron's axial frequency is equivalent to shifting the frequency of the parametric drive upward to point C in the figure. The electron's axial motion remains unexcited during the initial (and critical) cyclotron excitation, until the electron enters the single-valued region at arrow B enroute to point C. Even when the axial frequency shifts back because the cyclotron drive is turned off, the parametric hysteresis makes the ax-

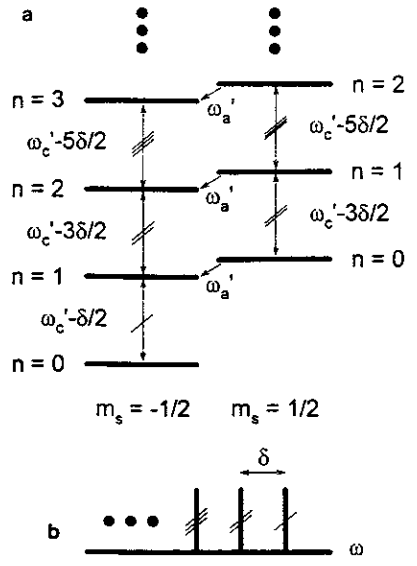

Fig. 18. **a** Energy eigenstates (number states) for the relativistic electron-cyclotron oscillator, with cyclotron quantum number n and spin quantum number m_s. **b** Corresponding transition frequencies

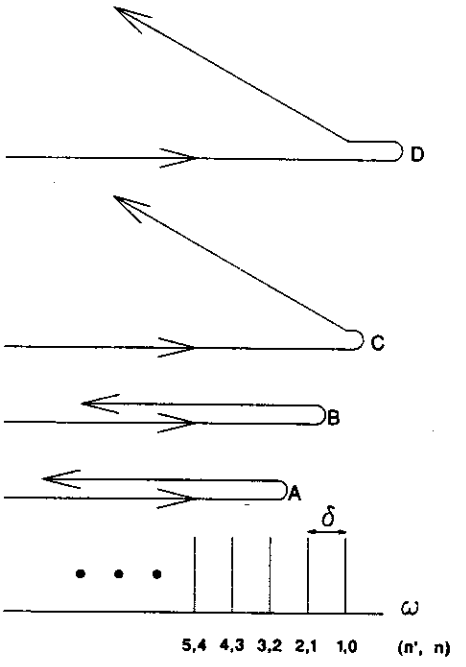

Fig. 19. Representation of the change in the frequency of the drive applied to excite the cyclotron motion of an electron (*above*) in comparison to the resonant frequencies (*below*). For a cyclotron motion initially in its ground state, sweeping the drive to the "turning points" in A or B produces no excitation, whereas sweeping to the turning points C or D allows a large excitation

ial excitation persist, as indicated by point D in the figure. The FET detector is subsequently turned on to read out the one-bit memory, to find out whether an axial frequency shift (and hence a cyclotron excitation) took place.

The energy levels for the lowest cyclotron eigenstates (number states) are shown in Fig. 18. Since no spin is flipped, we focus on one of the two "ladders" of Landau levels. Because of special relativity, the cyclotron energy levels are not equally spaced. Instead, the transition frequency between successively higher pairs of energy levels is lower by

$$\delta = \frac{\hbar(\omega_c')^2}{mc^2}\,, \tag{9}$$

where $\delta/\omega_c' = 10^{-9}$. To make a cyclotron excitation, a cyclotron drive frequency is swept upward to a turning point and then back downward [9, 13], as illustrated in Fig. 19. If the turning point is higher in frequency than the unshifted cyclotron frequency (C and D in Fig. 19), a large excitation is expected (like that directly detected with the FET turned on, in Fig. 16). If the turning point is less than the unshifted cyclotron frequency (and there is no power broadening), then no excitation is expected (A and B in Fig. 19). Figure 20 shows the probability of observing a large excitation as a function of turning-point frequencies which are separated from each other by one part in 10^9 (1 ppb). Each point is the average of 10 trials. It took two hours to produce this curve owing largely to the time required to turn on and off the heavily filtered voltage supply for the FET. The observed edge is very clean and has a resolution width less than 1 ppb. This is gratifying insofar as 1 ppb corresponds to the relativistic frequency shift due to a single-quantum excitation of the cyclotron oscillator. We have thus succeeded in resolving a one-quantum excitation of the cyclotron motion using special relativity, without resorting to any magnetic-field inhomogeneities which couple the various electron motions and severely broaden the resonance line shapes [5, 14]. This

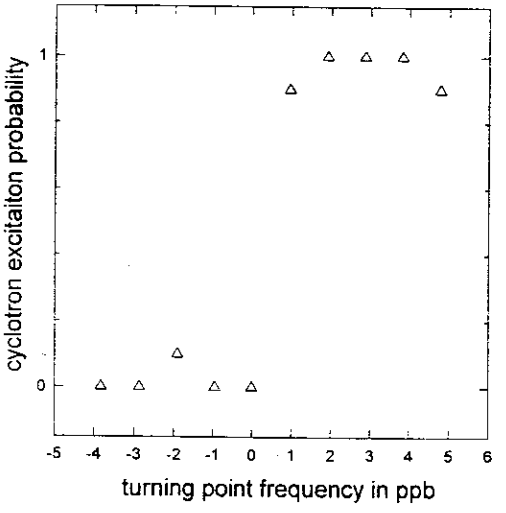

Fig. 20. Probability for "pulled" relativistic excitation of the cyclotron motion of one electron as a function of the turning-point frequency from which the cyclotron drive is swept to lower frequencies

resolution also indicates that the magnetic field produced by a self-shielding, superconducting solenoid [15] drifted less than 1 ppb during this particular 2 h measurement.

For a completely "in the dark" experiment, the axial motion must also be decoupled from the thermal noise from the detection resistor. This is easily accomplished by detuning the trap potential to make the axial frequency no longer resonant with the *LCR* circuit which the resistor in Fig. 3 represents. However, the axial excitation will remain at the average energy corresponding to 4.2 K insofar as such detuning also eliminates the axial damping. To cool the axial

motion below 4.2 K, it should be possible to employ cavity side-band cooling [16]. At the 4.2 K ambient temperature of our current traps, the cooling limit for the axial motion would be 2 mK. If we succeed in lowering our ambient temperature to 20 mK (an apparatus without the trap installed has already reached 17 mK), then the axial energy would be reduced to only 9 μK.

4 Conclusion

We look forward to repeating these studies in a cylindrical Penning trap [17], where the radiation modes are now well measured and understood [8, 18]. Observing a clean parametric resonance will be somewhat more difficult owing to the larger trap anharmonicity represented by the parameter C_6 and may require a specially designed cylindrical Penning trap in which C_6 is very small. The "in the dark" techniques demonstrated here, together with the desireable properties of the cylindrical Penning trap, suggest the likelihood of a new generation of electron g-2 measurements with higher accuracy and smaller systematic errors. Observing clean parametric resonance with a single electron also demonstrates the sensitivity required to study the nonlinear dynamics of two, three, four and more interacting electrons. An initial study of the collective plasma behavior of many trapped electrons has been carried out [8], and now it should be possible to study the onset of collective motions as the particle number is increased from unity.

Acknowledgements. We are grateful to D. Enzer for experimental assistance and for comments on this report. This work was supported by the National Science Foundation and the Office of Naval Research.

References

1. See review by L.S. Brown, G. Gabrielse: Rev. Mod. Phys. **58**, 233 (1986)
2. L.D. Landau, E.M. Lifshitz: *Mechanics*, 3rd edn. (Pergamon, New York 1976) p. 27
3. G. Gabrielse, X. Fei, L.A. Orozco, R.L. Tjoelker, J. Haas, H. Kalinowsky, T.A. Trainor, W. Kells: Phys. Rev. Lett. **65**, 1317 (1990)
4. D. Wineland, P. Ekstrom, H.G. Dehmelt: Phys. Rev. Lett **31**, 1279 (1973)
5. R.S. VanDyck, Jr., P.B. Schwinberg, H.G. Dehmelt: Phys. Rev. Lett. **59**, 26 (1987)
6. T. Kinoshita, D.R. Yennie: In *Quantum Electrodynamics*, ed. by T. Kinoshita (World 1990) p. 1
7. G. Gabrielse: Phys. Rev. A **27**, 2277 (1983)
8. J. Tan and G. Gabrielse: Phys. Rev. Lett. **67**, 3090 (1991); Phys. Rev. A. **48**, 3105 (1993)
9. G. Gabrielse, H.G. Dehmelt, W. Kells: Phys. Rev. Lett. **54**, 537 (1985)
10. G. Gabrielse, H.G. Dehmelt: Phys. Rev. Lett. **55**, 67 (1985)
11. L.S. Brown, G. Gabrielse, K. Helmerson, J. Tan: Phys. Rev. Lett. **55**, 44 (1985); Phys. Rev. A **32**, 3204 (1985)
12. G. Gabrielse, J. Gröbner, W. Jhe, H. Kalinowsky, D. Phillips, W. Quint: Nucl. Phys. A **558**, 701c (1993)
13. H. Dehmelt: Ann. de Phys. (Paris) **10**, 777 (1985)
14. R. Mittleman, F. Palmer, G. Gabrielse, H.G. Dehmelt: Proc. Nat'l Acad. Sci. USA **88**, 9436 (1991)
15. G. Gabrielse, J. Tan: J. Appl. Phys. **63**, 5143 (1988)
    G. Gabrielse, J. Tan, P. Clateman, L.A. Orozco, S.L. Rolston, C.H. Tseng, R. Tjoelker: J. Magn. Reson. **91**, 564 (1991)
16. G. Gabrielse: In *Laser Manipulation of Atoms and Ions*, ed. by E. Arimondo, W.D. Phillips, F. Strumia (North-Holland, New York 1992) p.631
17. J. Tan, G. Gabrielse: Appl. Phys. Lett. **55**, 2144 (1989)
18. G. Gabrielse, J. Tan: In *Cavity Quantum Electrodynamics*, ed. by P.R. Berman (Academic, New York 1994) p.267